Journal of Marine Research, 68, 851–880, 2010

Breaking internal waves and turbulent dissipation

by S. A. Thorpe[1,2]

ABSTRACT

We explore what might be discovered about the breaking of progressive internal waves and the consequent mixing by following some of the methodologies and techniques used to study surface wave breaking. It is suggested that breaking is most likely to occur in wave groups, where the wave field is locally amplified. In a stratified fluid of uniform buoyancy frequency, N, the breaking regions of internal wave groups extend in approximately horizontal directions. Two classes of breaking, "convective overturn" and "shear instability," are possible in progressive internal waves propagating in uniform stratification with no mean shear. Convective overturning and associated static instability occur at all wave frequencies, but only if the wave slope, $s = am$, exceeds unity, where a is the wave amplitude and m is the vertical wavenumber. Self-induced shear instability may take place in waves with slopes $s < 1$, and therefore less than the slopes required for convective overturn, but only when a wave-related Richardson number is sufficiently small; to achieve this, the wave frequency must be close to the inertial frequency. Equations are derived to express the energy dissipated in breaking or the strength of breaking in terms of the characteristics of a breaking wave. A particular measure of breaking analogous to that used to quantify surface wave breaking is $\Lambda_{\mathrm{I}}(c_b)dc_b$, the mean area of the fronts of breaking regions, projected onto the vertical and per unit volume, that are produced by internal breakers traveling at speeds between c_b and $c_b + dc_b$. Estimates are made of the values of Λ_{I} required to sustain a vertical eddy diffusion coefficient of $K_\rho = 10^{-5}\ \mathrm{m^2\,s^{-1}}$ through the breaking of internal waves of typical amplitude by convective overturn (with $s > 1$) and by the self-induced shear instability of near-inertial waves when $s < 1$. Values of Λ_{I} are of order $1.0 \times 10^{-2}\ \mathrm{m^{-1}}$ (i.e., a vertical surface area of about 10 cm × 10 cm in each cubic meter). The predictions are tested by using them to find the fraction of the water column in which turbulence occurs and by comparing the predicted values with existing observations. Additional theoretical studies and laboratory experiments are required to test the proposed analytical relations. Existing sea-going measurement techniques are reviewed and further observations are suggested to advance the understanding of breaking internal waves.

1. Introduction

Breaking internal waves are a dominant mechanism of diapycnal mixing and diffusion in the ocean thermocline (Wunsch and Ferrari, 2004), but definitive observations linking waves to turbulence are lacking. Substantial advances have, however, been made in

1. School of Ocean Sciences, Bangor University, Menai Bridge, Anglesey LL59 5AB, United Kingdom.
2. Correspondence address: "Bodfryn," Glanrafon, Llangoed, Anglesey, LL58 8PH, United Kindgom. ***email: oss413@sos.bangor.ac.uk***

developing ways to quantify the effects of breaking of gravity waves on the sea surface. This is an exploration of what can be discovered about progressive internal wave breaking, turbulent mixing and diffusion, by applying methodologies and techniques similar to some of those used to study breaking surface waves.

A useful and powerful measure of the breaking of surface gravity waves in deep water introduced by Phillips (1985), is $\Lambda(c)dc$, the mean crest length of breakers per unit surface area traveling with speeds between c and $c + dc$. Phillips predicts that $\Lambda \propto c^{-6}$ in the equilibrium range of the surface wave spectrum. Moments of the integral of $\Lambda(c)$ are written as $\int c^{\mathrm{n}}\Lambda(c)dc$, where the power, n, indicates the order of the moment, and these provide measures of the consequences of breaking. For example the zero moment with $\mathrm{n} = 0$ gives the total length of breakers per unit surface area, the first moment with $\mathrm{n} = 1$ gives the fraction of sea surface that is broken (or "turned over") per unit time, and $\tau_{\mathrm{p}}\int c\Lambda(c)dc$ is the fractional "active" whitecap coverage if the foam bubbles produced by a breaker persist of a fixed time, τ_{p}. ("Active" denotes foam patches in the process of being generated by breaking waves.) Alternatively, if foam bubbles persist for a time equal to a constant, r, times the wave period, $T = 2\pi cg^{-1}$, where g is the acceleration due to gravity, the expression $(2\pi rg^{-1})\int c^2\Lambda(c)dc$, proportional to the second moment, gives the fractional active whitecap coverage.

Duncan (1981) proposes a dimensionally correct formulation for the rate of dissipation of wave energy per unit crest length of a breaking wave:

$$\varepsilon_{\mathrm{I}} = b\rho c^5 g^{-1}, \tag{1}$$

where b is a nondimensional number estimated from Duncan's laboratory experiments to be about 0.06, ρ is the density of water and c is the "speed of the breaker," and it follows from (1) that the fifth moment of Λ is proportional to the rate of loss of energy per unit area from the surface waves through their breaking. (There are differences in the definition of c, it being sometimes defined as the phase speed, c_*, of linear waves in a group that contains a breaker, and more commonly as the speed of the wave that is breaking, c_b, taken to be equal to the speed of advance of the front of the whitecap formed in the breaking process. Banner and Pierson (2007) find that $c_b/c_* = 0.9 \pm 0.05$, whilst Tian *et al.* (2010) find $c_b/c_* = 0.9 \pm 0.1$. We shall later adopt the speed of advance of a breaker zone, c_b, in the formulation of a dissipation rate.)

The number b is sometimes called the "wave breaking strength parameter" (e.g. Tian *et al.,* 2010) and may not be constant. It is estimated by Drazen *et al.* (2008) to lie in the range, 10^{-3}–10^{-1}. Assuming an inertial scaling for turbulence generated in a plunging (or convectively overturning) breaker, so that the rate of dissipation of turbulent kinetic energy per unit mass, ε, is proportional to (u^3/l), where u is a velocity scale and l is a length scale, Drazen *et al.* predict (and, through laboratory experiments, test and give support to) a relationship $b = \beta(hk)^{5/2}$, where β is a constant of order unity and hk is a measure of the local slope of a wave at breaking. Better agreement with laboratory experiments is found by taking $b \propto S^{2.77}$, where S is an integral measure of the maximum

wave slope in the wave group containing the breaking wave; see also Banner and Peirson, 2007; Tian *et al.,* 2010. These authors also develop and test another formulation to predict the breaking of waves in a group, based on a parameter, δ, that is proportional to the rate of change, following the group, of a nondimensional measure of the energy density of its component waves. We shall not further discuss or extend this particular formulation to internal waves because it introduces rates that are extremely difficult, if not impossible, to determine through measurements within the ocean.

Following earlier studies by Melville and Madusov (2002) off the coast of North Carolina, Kleiss and Melville (2010) use a video camera flown in an aircraft over the Gulf of Tehuantepec to obtain images of surface wave breakers from which, using analytical methods developed by Kleiss and Melville (2011), they determine the speed and length of breaking waves producing foam patches, and hence Λ. They also examine the variation of a nondimensionalized form of Λ with a variety of nondimensional measures, such as fetch and wave age. Rather than being proportional to c^{-6} as predicted by Phillips (1985), Kleiss and Melville find that $\Lambda(c)$ can best be described by a Rayleigh distribution.

The breaking of surface waves is made visibly evident by the formation of foam and whitecaps. In contrast, the breaking of internal waves in the ocean is hidden from sight and therefore relatively obscure being, in general, only evident through the presence of turbulent microstructure measured by, e.g., free-fall probes. There are many reports of patches of turbulence within the ocean thermocline (e.g., Grant *et al.,* 1968; Gregg, 1980; Gregg and Sanford, 1988; Alford and Pinkel, 2000). In the deep ocean, internal wave breaking is thought to be one of the main causes of the turbulent patches, leading to substantial diapycnal mixing (Munk, 1966; Wunsch and Ferrari, 2004) but the time-history of the patchy turbulent events, from their onset to decay or turbulent collapse, and hence their relation (if any) to internal waves, is almost unknown. (A notable exception is the observations by Woods, 1968, of Kelvin-Helmholtz instability, KHI, in association with internal waves on a thin density interface, but even here there is little supporting evidence to quantify the onset, speed, frequency or extent of the breaking events.)

What might be learnt about turbulent energy dissipation in the stratified ocean from a study, analogous to that of breaking surface waves but applied to breaking internal gravity waves, and what additional information is needed to apply the methodology to examine and quantify mixing within the ocean? The first question is addressed in Sections 2–5 and the second in Section 6. This includes a brief review of existing measurement techniques and, in Section 6d, a proposal for novel observations in the main thermocline.

2. Internal waves in a uniformly stratified ocean

Of the various types of internal waves, waves at the interface between two layers of uniform density (which includes the density model often used in the study of large amplitude, nonlinear, soliton-type, internal waves or NLIWs) are most akin to the surface waves, except that breaking of progressive interfacial waves is more likely to occur as a consequence of KHI rather than by convective overturn (Fringer and Street, 2003; Troy

and Koseff, 2005; Fructus *et al.,* 2009; Barad and Fringer, 2010; see also Moum *et al.,* 2003). Although extension of the findings for surface waves to these interfacial internal waves may be more direct, we choose instead to examine progressive internal waves in a continuous and uniformly stratified rotating fluid, a particular interest being in internal wave groups propagating through the main ocean thermocline. Careful observation of the occurrence and repetition of wave-produced foam patches or whitecaps appearing on the sea surface (e.g., Donelan *et al.,* 1972) suggests that there the breaking of waves in groups is common and may be dominant in the process of the entrainment of air across the water surface, from the atmosphere into the sea. It is likely that the breaking of internal waves in wave groups will determine where and how diapycnal mixing occurs most frequently *within* the ocean. Alford and Pinkel's (2000) observations from R/P *FLIP* of the co-location of statically unstable regions and internal wave packets support this notion. The groups observed in local regions within the body of the ocean may be generated, for example, by transient wave forcing at the foot of the mixed layer or as a consequence of the process of a cascade of energy driven by wave interactions (Staquet and Sommeria, 2002). If of particular shape (Thorpe, 2010) or frequency band-width (e.g., Thorpe, 2002) the groups may remain coherent for several times the period of their dominant waves.

We follow Duncan's formulation, (1), but define a new quantity, ε_I, the rate of dissipation of wave energy per unit breaking crest length per unit breaker height in internal waves.[3] The dimensions of ε_I are $(ML^2T^{-2})T^{-1}(L^{-2}) = MT^{-3}$ (where M = mass, L = length and T = time) and, for simplicity ignoring the complexity of, e.g., the energetics of an ambient wave field, the available dimensional quantities are a reference density, ρ_0, the buoyancy frequency, N, the Coriolis parameter, f, and c_b, the speed of the breaking wave. A dimensionally correct equation is

$$\varepsilon_I = \rho_0 c_b^3 B(J_i), \tag{2}$$

where B is an internal wave breaking strength parameter analogous to b in (1) and a function of nondimensional wave parameters, J_i, that characterize breaking. These parameters may include the local wave-induced value of the Richardson number, the wave propagation direction relative to the horizontal, the steepness, s, of the breaking wave, and the parameter, $F = f/N$, or some combination, as discussed below. The Richardson number characterizing the mean flow through which waves are traveling might be a further nondimensional parameter, but (again for simplicity, except when briefly mentioned in Section 7) we suppose the background mean shear is small in comparison with that generated by the waves and the "background" Richardson number is so large that mean

3. In analogy with surface waves, it is natural, as here, to define ε_I as the rate of energy loss to turbulence per unit breaking crest vertical area and later to define Λ_I as the mean vertical area of the leading edge of an internal breaker per unit volume. Taking ε_I as the rate of dissipation per unit breaking crest length per unit horizontal area (as for surface waves) and not introducing a vertical dimension into the metric leads to problems in finding the rate of dissipation of turbulent KE per unit volume.

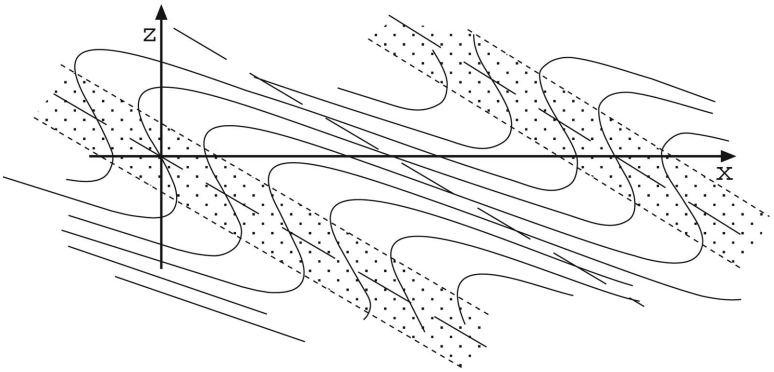

Figure 1. A statically unstable, convectively overturning internal wave in a fluid of constant N. Isopycnal surfaces for internal waves are shown when $s = 1.5$ and $\theta = \pi/6$. Stippled regions are statically unstable. The dashed lines are at angle θ to the horizontal and indicate lines of constant phase, parallel to which the group velocity, c_g, is directed (from Thorpe, 1994b, Fig. 2).

shear does not affect the breaking process. The buoyancy frequency, N, does not appear explicitly in (2), but its importance will soon be evident.

If it is assumed that breaking occurs in wave groups propagating in the x (horizontal) and z (vertically upward) plane, then the vector speed of a breaking region is the sum of the wave phase velocity, $\underline{c}$, and the group velocity, $\underline{c}_g$,

$$\underline{c}_b = \underline{c} + \underline{c}_g, \tag{3}$$

(Thorpe, 1999a). This is a vector that is exactly horizontal if the wave frequency is large compared with f (Phillips, 1966; his Fig. 5.7), and not far from horizontal for near-inertial waves. The speed $c_b = N/K$, where K is the magnitude of the wavenumber of the internal wave. (The theory is reviewed in Appendix A). Hence from (2):

$$\varepsilon_I = \rho_0 c_b^3 B(J_i) = \rho_0 (N/K)^3 B(J_i). \tag{4}$$

But how to find the breaking strength parameter, $B(J_i)$? Two mechanisms of internal wave breaking are known to lead to the production of turbulence (e.g., see Liu *et al.,* 2010), and these are dealt with separately in the next two sections.

3. Static instability; convective overturn

Convective overturn leading to static instability, illustrated in Figure 1 and first identified as a breaking mechanism by Orlanski and Bryan (1969), is possible only when the wave slope, $s = am$, of internal waves exceeds unity, where a is the wave amplitude (the amplitude of isopycnal displacements) and m is the vertical wavenumber. Convective instability will follow provided the Rayleigh number, Ra, of the overturning region defined in Appendix B (A13) is sufficiently large; see also Section 6a. Supposing an inertial scaling

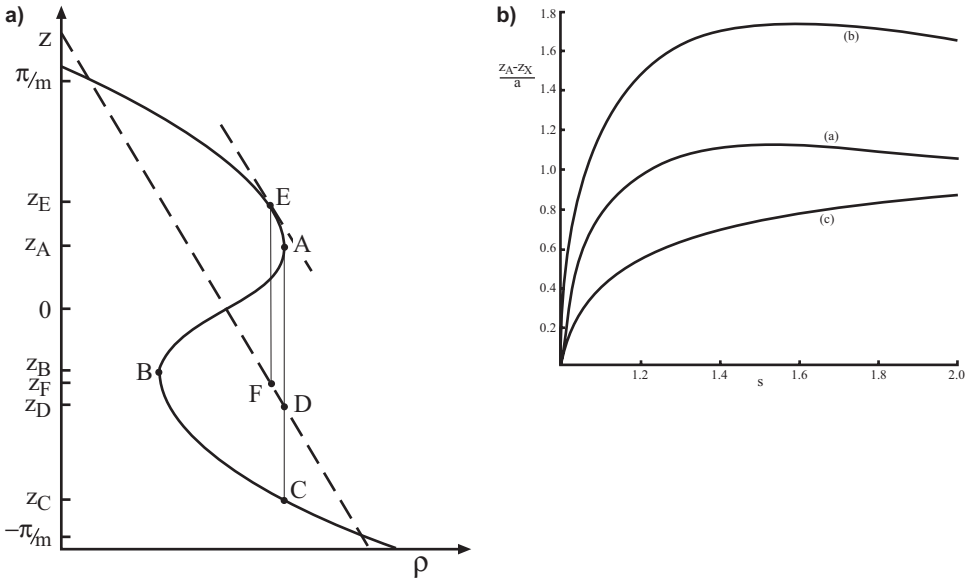

Figure 2. (a) The density profile at $x = t = 0$ when $s > 1$. A, at level z_A, indicates a density maximum and B, at level z_B, the first density minimum below A. The vertical density gradient is positive and the fluid statically unstable in AB. The point C has the same density as A and z_C marks the level to which fluid of the density at A might sink in a static fluid without density change. The level z_D is the location of fluid of density A in the "undisturbed" density profile, $\rho = \rho_0(1 - N^2 g^{-1} z)$, shown by the dashed line through F and D. The dashed line tangential to the density profile at E is parallel to $\rho = \rho_0(1 - N^2 g^{-1} z)$; the distance EF $= a$ is the maximum displacement from the "undisturbed" profile resulting from the presence of the internal wave (see Appendix B). (b) Variation of wave properties with wave slope, $s = am$. Curves are labeled (a)–(c) where in (a) $z_X = z_B$: $(z_A - z_B)/a = 2s^{-1}\cos^{-1}(s^{-1})$ (equal to h/a and giving the height of the statically unstable region; see A9); in (b) $z_X = z_C$: $(z_A - z_C)/a$ giving the distance over which fluid might sink, retaining its density (see A10 and A11); and in (c) $z_X = z_D$: $(z_A - z_D)/a = (s^2 - 1)^{1/2} s^{-1}$ (see A12).

as do Drazen *et al.* (2008) for surface waves, the rate of dissipation of turbulent kinetic energy per unit mass within an unstable overturning breaker in a stratified region, ε, is equal to qu^3/h, where u is the velocity scale characterizing the turbulent motion and q is a nondimensional constant of order unity, and h is the height of the overturning region (the vertical distance between A and B in Figure 2a). (An alternative formulation for ε based on the Ozmidov length scale, but judged less sound, is described in Appendix C. In a particular example described in Appendix C we also compare the rate of dissipation of turbulent kinetic energy produced by the collapse of an overturn with that necessary to maintain eddies of Ozmidov scale in a turbulent fluid.) The rate of dissipation of turbulent kinetic energy per unit crest length and per unit breaker height is then

$$\varepsilon_I = q\rho_0(u^3 h^{-1})l, \tag{5}$$

where l is now the extent of the breaking region in direction $\underline{c}_b$. We suppose that the turbulent motion is dissipated in a time scale of rN^{-1}, where $r \approx 6$ (Smyth *et al.,* 1997), so that $l = rN^{-1}c_b = rK^{-1}$.

Assuming that the convectively unstable overturns collapse, transferring their potential energy into turbulent kinetic energy characterized by velocity u (that is subsequently dissipated in homogenizing the initially unstable region), we have $\rho_0 u^2 h/2 \approx$ PE, where PE is the potential energy per unit area of the overturning region relative to its mid level, $z = 0$ in Figure 2a, as given by (A14) of Appendix B. As shown in (A9), $h = 2as^{-1}\cos^{-1}(s^{-1})$, and we find $u^2 \approx (Na)^2 G(s)$, as in (A15), where G is a nondimensional function of the slope, $s = am$, given by (A16). Using (5), the rate of loss of energy per unit crest length per unit height is then

$$\varepsilon_I = q\rho_0 u^3 (l/h) \approx qr\rho_0 (Na)^3 G^{3/2} \cos\theta [2\cos^{-1}(s^{-1})]^{-1}, \tag{6}$$

where θ is the direction of group propagation (the angle between $\underline{c}_g$ and the horizontal), and where the relation, $k = m \tan\theta = K \sin\theta$, between the wavenumber, K, and its horizontal, k, and vertical, m, components has been used. The rate of energy loss is equal to $\rho_0 (N/K)^3 \mathrm{B}(J_i)$ in (4), if

$$B(J_i) = qrs^3 G^{3/2} [2\cos^{-1}(s^{-1})]^{-1} \cos^{-2}\theta \tag{7}$$

using $K = m/\cos\theta$, or

$$B(J_i) = qrH(s)\cos^{-2}\theta(2\pi)^{-1}, \tag{8}$$

where $r \approx 6$ and

$$H(s) = \pi[2\{3(s^2 - 1)^{1/2} - 3\cos^{-1}(s^{-1}) - [\cos^{-1}(s^{-1})]^3\}/3]^{3/2}[\cos^{-1}(s^{-1})]^{-5/2}. \tag{9}$$

The value of q is unknown and is probably a function of the Reynolds and Rayleigh numbers of the convective overturns (Section 6a).

The functions $G(s)$ and $H(s)$ are shown in Figure 3. The term $(\cos\theta)^{-2}$ in (7) may be large, and so may $B(J_i)$, when $\theta \sim \pi/2$ (i.e., for waves of frequency near N).

The breaking strength parameter for breaking through convective overturn, B, is therefore determined from (8) and (9) in terms of s and θ. If, for example, $s = 1.5$, $q \approx 1$ (but see Section 6a) and $\theta = \pi/6$ (as in Fig. 1),

$$\varepsilon_I \approx 0.074\rho_0 (Na)^3. \tag{10}$$

(If, instead of allowing convection to occur from z_B to z_A in Figure 1a, we take convection over the distance $2|z_C|$, the greatest range of z over which gravitational instability might occur, where z_C is given by (A11), then (10) becomes $\varepsilon_I \approx 0.078\rho_0 (Na)^3$; the sensitivity of ε_I to the distance over which convection occurs is relatively small.)

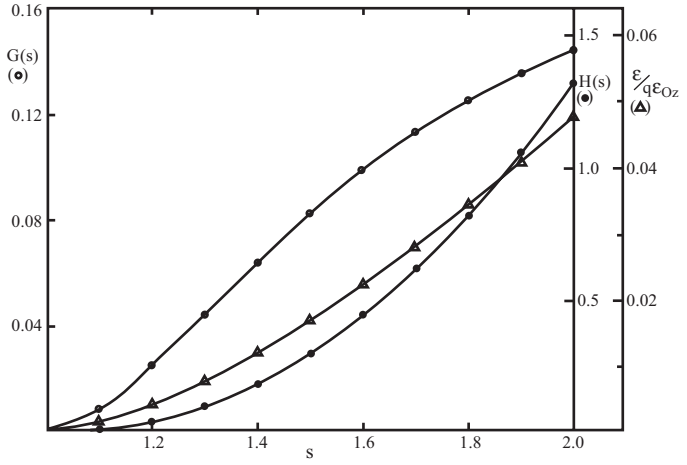

Figure 3. The functions $G(s)$ (circles; giving u^2; see A15, A16), $H(s)$ (dots; giving the breaking strength of convectively breaking waves, $B(J_i)$; see (8) and (9)), and $s^3G^{3/2}[\cos^{-1}(s^{-1})]^{-3}/8$ (triangles, giving $\varepsilon(q\varepsilon_{Oz})^{-1}$; see A17).

4. Shear instability

Self-induced Kelvin-Helmholtz shear instability (KHI) was identified as a cause of internal wave breaking by Phillips (1966) and may occur at a lower value of s than convective overturn (i.e., at a slope $s \leq 1$). In a uniform density gradient it can, however, occur only in near-inertial waves, waves that create shear and strain the fluid, so changing the vertical density gradient. Instability is most likely to set in when the wave-induced gradient Richardson number based on the shear in the x-direction of wave propagation, Ri_x, falls below ¼ (Thorpe, 1999b). The horizontal wavelength of the disturbance that first becomes unstable is about $1.17(2\pi m^{-1})$, where m is the vertical wavenumber of the internal wave. Kunze *et al.* (1990b) attribute regions of low Ri observed using a neutrally buoyant float mainly to near-inertial waves, whilst billows associated with near-inertial waves in the seasonal thermocline of the Sargasso Sea are reported by Marmorino (1987) and Marmorino *et al.* (1987). There appear, however, to be no analytical or laboratory studies of breaking near-inertial waves in a uniformly stratified fluid (like those, for example, of Fringer and Street, 2003, and Troy and Koseff, 2005, for KHI generated by waves on a narrow interface without rotation); there is no information about the minimum, wave induced, Richardson number that is required before billow overturn and mixing set in, or about the energy that is then lost through turbulence. It is therefore necessary to adopt three assumptions about the breaking of internal waves in uniform stratification:

Fringer and Street (2003) suggest that a gradient Richardson number $Ri \sim 0.13$ is needed for billows caused by internal waves traveling along a broad interface. Troy and Koseff (2005) find a corresponding Ri of (0.07–0.08) ± 0.03. It is therefore first assumed that (although instability may occur at larger values of the Richardson number) Ri_x must be

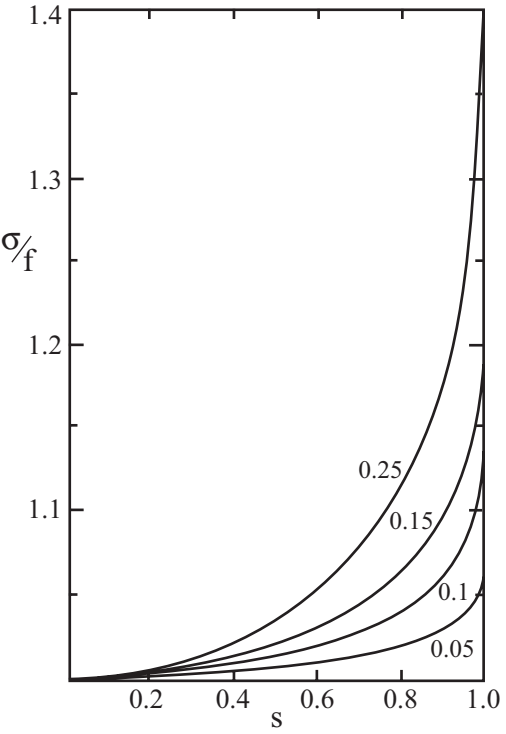

Figure 4. The relation of σ/f and s when the minimum Richardson number in the wave-induced flow is equal to 0.05, 0.1, 0.15 and 0.25, and when $F = 0.1$.

at least as small as a value $Ri_{xc} \sim 0.1$ for billow mixing to set in. Setting Min $Ri_x = Ri_{xc}$ gives a relation between θ, F and s (Eq. A23 in Appendix D); Figure 4 shows the values of s and σ/f at which the Richardson number in the wave-induced flow first reaches 0.05. 0.1, 0.15 and 0.25. (Here σ is the wave frequency and f the Coriolis parameter.)

Secondly, it is supposed that the billows will cause mixing, quickly homogenizing the region that extends upward and downward from the level z_0 where $Ri_x = Ri_{xc}$ to those where $Ri_x = 1/4$, (levels z_1 and z_2), resulting in uniform density and velocity in the region. This implies that mixing extends rapidly (compared to c_b) throughout the region where $Ri_x < ¼$ at the time and x-location where $Ri_x = Ri_{xc}$. Nondimensional heights ζ_0, ζ_1 and ζ_2, where $\zeta_i = mz_i$, are shown in Figure 5.[4] The difference between the kinetic energy lost and the potential energy gained per unit volume in this mixing process, $\Delta = \rho N^2 m^{-2} A(s, F, Ri_{xc})$ (A28), provides an estimate of the energy available to the turbulent

4. Because, in general, neither the velocity nor the density profile is symmetrical in z_1 to z_2, the sometimes-adopted way of representing the state after instability by linear profiles of velocity components and density with no discontinuities in shear at z_1 and z_2 (e.g., Polzin, 1996) will not conserve mass and momentum. We therefore, for simplicity, choose a homogenized state.

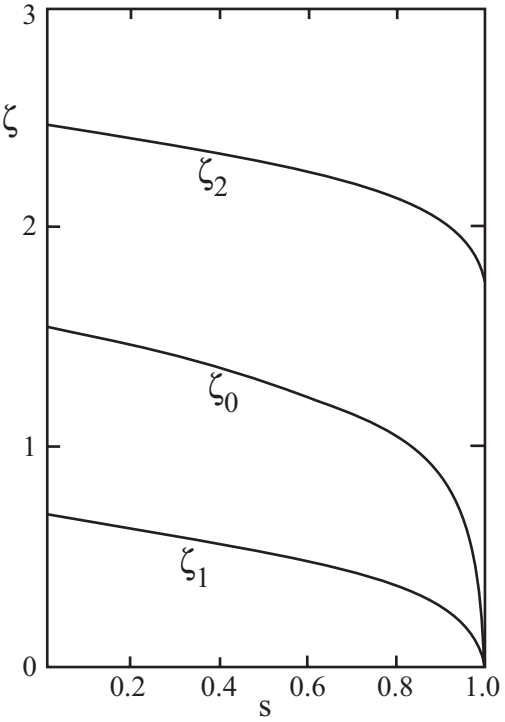

Figure 5. The values of ζ_0, ζ_1 and ζ_2, when $F = 0.1$ and $Ri_{xc} = 0.1$ (see Appendix D).

motion induced by the billows, where the function $A(s, F, Ri_{xc})$ is shown in Figure 6 for $F = f/N = 0.1$, and $Ri_{xc} = 0.05$, 0.1 and 0.15. $A(s, F, Ri_{xc})$ is evidently sensitive to the selection of Ri_{xc}, but varies little with s for $s \leq 0.4$; further details are given in Appendix D.

Finally, it is assumed that turbulence decays within a time $\tau = rN^{-1}$ in which the breaking front moves forward a distance $c_b rN^{-1}$, so that, as in Section 3, the mixing occurs over a length $l = rK^{-1}$. The turbulent decay rate is then $\Delta\tau^{-1}$ and the rate of dissipation per unit breaking crest length per unit crest height is

$$\varepsilon_I = \rho_0 N^3 m^{-3} A(s, F, Ri_{xc}) \cos\theta, \tag{11}$$

using $K = m(\cos\theta)^{-1}$, as in (A29). The length of breaking, $l = rK^{-1}$, divided by the billow wavelength, $2\pi \times 1.17m^{-1}$, is equal to about $5.1 \cos\theta \approx 5.1$ since, for the near-inertial waves, θ is small.

The breaking strength parameter is determined by comparing (4) and (11):

$$B(J_i) = A(s, F, Ri_{xc}) \cos^{-2}\theta. \tag{12}$$

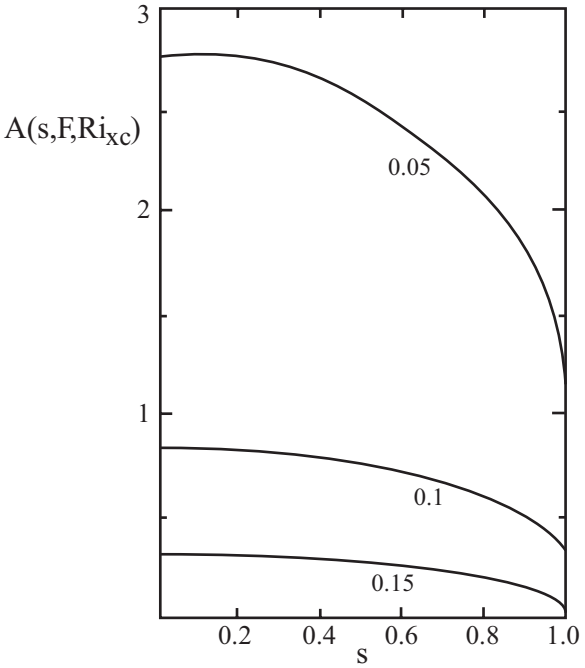

Figure 6. The function $A(s, F, Ri_{xc})$ when $F = 0.1$ and when $Ri_{xc} = 0.05$, 0.1 and 0.15, as labeled. $A(s, F, Ri_{xc})$ is related to the energy lost to turbulence per unit volume: from (A28), $A(s, F, Ri_{xc}) = m^2(\text{KE-PE})[\rho_0 N^2(z_2 - z_1)]^{-1}$.

Writing (11) as $\varepsilon_I = \rho_0(Na)^3 s^{-3} A(s, F, Ri_{xc})\cos\theta$ and if, for example, $F = 0.1$, $s = 0.4$, and $Ri_{xc} = 0.1$ (when $\sigma/f = 1.0084$ from Figure 4 and $\theta = 0.746$ deg. from (A21)), and taking the appropriate value of $A \approx 0.78$ from Figure 6:

$$\varepsilon_I \approx 12.2\rho_0(Na)^3. \tag{13}$$

This exceeds the value found in the example taken to illustrate the dissipation in convective overturn, (10), provided the values of Na are supposed equal.

5. Values of Λ_I

A measure of internal wave breaking, akin to $\Lambda(c)dc$ used for surface waves, is $\Lambda_I(c_b)\mathrm{d}c_b$, the area (projected onto the vertical and per unit volume) of the fronts of breaking regions produced by internal breakers traveling at speeds relative to the surrounding fluid between c_b and $c_b + dc_b$. (It will be noticed that since the breaking regions are nearly horizontal—see comment below (3)—it may be sufficient to make measurements of the crest length per unit isopycnal surface area to determine the mean dissipation as for surface waves; but see footnote 3.) Using the relation (6) for ε_I, the rate of dissipation of

turbulent kinetic energy per unit mass of a convectively overturning breaker moving at speed c_b is

$$\varepsilon = \Lambda_I \varepsilon_I / \rho_0 = qr\Lambda_I (Na)^3 G^{3/2} \cos\theta [2\cos^{-1}(s^{-1})]^{-1}. \quad (14)$$

A commonly used relation for the diapycnal diffusivity is

$$K_\rho = \Gamma \varepsilon N^{-2} \quad (15)$$

(Osborn, 1980), where Γ is an efficiency factor, about 0.2. If we suppose that all the mixing is a consequence of convective overturn, we can use (14) and (15) to derive $K_\rho = \Gamma qr\Lambda_I Na^3 G^{3/2} \cos\theta [2\cos^{-1}(s^{-1})]^{-1}$, or rearranging

$$\Lambda_I = 2K_\rho \cos^{-1}(s^{-1}) (\Gamma qrNa^3 G^{3/2} \cos\theta)^{-1}. \quad (16)$$

The factor Λ_I required to support a given value of K_ρ by waves of amplitude a and slope s traveling in direction θ through the main thermocline with buoyancy frequency, N, can now be determined. Observations by Gregg (1980) of temperature microstructure in the main thermocline of the subtropical gyre of the North Pacific at depths of 800 m to 1200 m, a depth range stable to double-diffusive instabilities, are used to provide "typical" values. The buoyancy frequency is about $N = 5 \times 10^{-4}$ s^{-1}, turbulence (determined from the microstructure measurements of zero-crossings of temperature gradients) occupied a fraction, Q (used later), ranging from about 0.07 to 0.36 of the water column. The size of overturns is typically about 5 m. (Gregg actually finds larger overturns, one as large as 7.5 m, but 5 m is chosen to be a representative value. Gregg and Sanford, 1988, find $Q \approx 0.14$ for "active" turbulence at depths of 500 − 1000 m in the eastern North Pacific, "active" meaning that $\varepsilon > 16\nu N^2$, a value below which the turbulent buoyancy flux becomes very small. In the same area, but at depths of 180–200 m, Kunze *et al.,* 1990b, find that the Richardson number measured at scales less than 2 m is less than 0.25 in a fraction 0.11 of the water column.) So if $K_\rho = 10^{-5}$ m^{2}s^{-1} is a mean "background level" (Gregg, 1989), supposed to be supported by convectively breaking internal waves with $h = 5$ m and $N = 5 \times 10^{-4}$ s^{-1}, and if (tentatively, see Section 6a) we choose $q \approx 1$ and $\Gamma = 0.2$,[5] then Λ_I given by (16) increases from 1.09×10^{-2} m^{-1} when $\theta = \pi/18$ (10 deg.) and $s = 1.6$ (so that, from (A9), $a = 4.47$ m and, from Figure 3, $G \approx 0.0993$), to 5.11×10^{-2} m^{-1} when $\theta = \pi/4$ (45 deg.) and $s = 1.2$ (when $a = 5.12$ m and $G \approx 0.0253$).

The parameter, Λ_I, the area of the fronts of *convectively unstable breaking* internal waves, projected onto the vertical and per unit volume, required to maintain a diapycnal diffusivity of 10^{-5} m^{2}s^{-1} has therefore values of about 1.1×10^{-2} m^{-1} to 5.1×10^{-2} m^{-1}. These values of Λ_I can be tested by using them to determine the fraction of the water column in which turbulence occurs, a value akin to the fractional cover of actively

5. This value appears to be valid in the range $7\nu N^2 < \varepsilon < 100\nu N^2$ (Shih *et al.,* 2005), but may overestimate K_ρ outside this range.

formed whitecaps in the surface wave regime. The fraction is Λ_I times the length of the turbulent region, rK^{-1},

$$Q = \Lambda_I ras^{-1}\cos\theta. \tag{17}$$

Substituting the above values of Λ_I at $s = 1.6$ and 1.2, with the corresponding values of θ and a, and with $r = 6$, gives $Q = 0.18$ and 0.93. The former is consistent with Gregg's observations but the latter is too great, suggesting that the higher values of Λ_I with the corresponding chosen values of h and s are too large.

Alternatively using the equation (11) for ε_I, the rate of dissipation of turbulent kinetic energy per unit volume resulting from shear instability is

$$\varepsilon = \Lambda_I \varepsilon_I/\rho_0 = \Lambda_I N^3 m^{-3} A(s, F, Ri_{xc})\cos\theta. \tag{18}$$

Supposing all the mixing is caused by shear instability and using (15), this can be written as

$$\Lambda_I = K_\rho m^3[(\Gamma NA(s, F, Ri_{xc})\cos\theta]^{-1}. \tag{19}$$

As before, we select $K_\rho = 10^{-5}$ m^2 s^{-1} and $N = 5 \times 10^{-4}$ s^{-1}, but now choose the extent, $z_2 - z_1$, of the region mixed by the billows to be equal to the 5 m extent of the overturns observed by Gregg (1980). Since $m(z_2 - z_1) = \cos^{-1}(8Ri_{xc} - 1)$ (Appendix D), the wave amplitude, $a = s(z_2 - z_1)[\cos^{-1}(8Ri_{xc} - 1)]^{-1}$. Choosing $Ri_{xc} = 0.1$, $F = 0.1$, and $\Gamma = 0.2$, we find that $s = 0.2$ gives $a = 0.56$ m, the vertical wavelength, $2\pi/m = 17.5$ m, $\sigma/f = 1.0017$ (from Fig. 4), $\theta = 0.336$ deg. (from A21), and $A(s = 0.2, F = 0.1, Ri_{xc} = 0.1) = 0.85$ (from Fig. 6), leading to $\Lambda_I = 5.45 \times 10^{-3}$ m^{-1}. Using (17), the fraction $Q = 0.09$, within the range found by Gregg. Choice of a larger slope, $s = 0.6$, gives $a = 1.7$ m, a vertical wavelength of 17.5 m, $\sigma/f = 1.0204$, $\theta = 1.169$ deg., $A(s = 0.2, F = 0.1, Ri_{xc} = 0.1) = 0.72$, and $\Lambda_I = 6.20 \times 10^{-3}$ m^{-1}. The fraction, $Q = 0.11$, is again within Gregg's range.

The parameter, Λ_I, required to maintain a diapycnal diffusivity of 10^{-5} m^2 s^{-1} through the *shear-induced breaking* of near-inertial internal waves ranges between typical values of about 5.4×10^{-3} m^{-1} to 6.2×10^{-3} m^{-1}. These are about half the values found for convective overturn, implying that shear-induced breaking is more effective in supporting mixing than convective overturn; less frequent shear breaking than convective overturn is needed to account for the observed oceanic mixing. It should be recalled, however, that whilst (16) applies to waves of all frequencies but with $s > 1$, (19) applies only to wave frequencies that are close to f with a specific relation (Fig. 4) between the frequency and the wave slope, s.

Garrett and Munk (1972) also conclude that waves breaking by shear instability are much more likely to account for ocean mixing than those breaking by convective overturn. In their formulation, the vertical eddy diffusion coefficient, K_ρ, is taken to be equal to $Z^2T_e^{-1}/12$, where Z is the vertical distance over which stratified fluid is (completely) mixed in each KHI event in breaking internal waves, and T_e is the average time interval between the occurrence of mixing events in a vertical distance, Z (see Garrett, 1979; his

Eq. 4.1). The use of (15) leads to $\langle \varepsilon \rangle = (5/12)\, Z^2 N^2 T_e^{-1}$, for the mean rate of dissipation of wave energy per unit mass by breaking internal waves.

The predictions draw attention to the value of measuring intermittency, the time interval between mixing events per unit depth and its relation to the breaking waves, e.g., to their frequency and slope, s.

6. What additional studies are suggested by the analysis?

The above are all rough "back of the envelope" estimates involving several assumptions, some of them "extreme" (e.g., in Section 4, that there is complete mixing following shear instability. This may result in a substantial overestimate of ε_I; Kunze *et al.,* 1990a). The proposed formulae should be tested (and if valid, used). There are numerous challenging problems. For example:

a. Will turbulent mixing occur following convective overturn?

This will depend on three nondimensional parameters characterizing the overturn: Ra, Pr and Re. A value of the Rayleigh number, Ra, exceeding about 10^2 appears sufficient for convective instability to occur in wave induced overturns (Thorpe, 1994a, Andreassen *et al.,* 1998, and Fritts *et al.,* 1998, describe numerical studies of the chain of instabilities and flow structures that follow the initial overturn and during the transition to turbulence.) In the laboratory, substantial mixing is observed following overturns in *standing* internal waves in which $Ra \sim 8 \times 10^7$ (accounting for a difference in the choice of the vertical scale in Ra) when the Prandtl number, Pr, ~ 700 (Thorpe, 1994b); critical values of Ra are likely to depend on both Pr and the Reynolds number, $Re = uhv^{-1}$ (Thorpe, 1994a). A value of Re of about 10^5 is required for the supposed inertial scaling, $\varepsilon = qu^3h^{-1}$, with $q \sim 1$, to be robust.

Figure 2b shows that $h \sim a$ when s is in the range $1.2 - 2.0$. Using this relation to express Ra and Re in terms of the overturning scale h, (A13) gives $Ra = N^2(s - 1)h^4(v\kappa)^{-1}$, and (A15) gives $Re = h^2 N G^{1/2} v^{-1}$, where, from Figure 3, $G^{1/2}$ ranges from 0.16 to 0.38. Taking typical "oceanic" values of buoyancy frequency, $N = (10^{-4} - 10^{-2})$ s^{-1}, overturning scale, $h = (1 - 10)$ m and kinematic viscosity $v = 1 \times 10^{-6}$ m^{2}s^{-1}, and diffusivity $\kappa = \kappa_T = 1.4 \times 10^{-7}$ m^2 s^{-1} (so $Pr \approx 7$) gives $Ra = 1.4 \times 10^4 - 7 \times 10^{10}$ and $Re = 1.6 \times 10^1 - 3.8 \times 10^4$. Although the Rayleigh number may be such that convective instability and subsequent mixing are likely, the assumption of an inertial range of turbulence when overturns are relatively small or when stratification is weak is not valid; the Reynolds number is not sufficiently high. The values $h = 5$ m and $N = 5 \times 10^{-4}$ s^{-1} chosen in making the estimates of Λ_I in Section 5 give $Ra = 6.7 \times 10^8$ and $Re = 3.9 \times 10^3$ when $s = 1.6$, and $Ra = 2.2 \times 10^8$ and $Re = 2.0 \times 10^3$ when $s = 1.2$; the values of Re are not large enough for inertial scaling following convective overturn and estimates of Λ_I with $q = 1$ must consequently be uncertain. Smaller values of q may be more appropriate. Further investigation is required

to establish a measure of dissipation in convectively overturning waves when Re is substantially less 10^5.

b. How to test the proposed formula for the breaking strength parameter, $B(J_i)$?

For surface waves, the size and variation of the nondimensional breaking strength parameter, b, in (1) is addressed through laboratory experiments (e.g., Duncan, 1981; Drazen *et al.,* 2008).

Although the convective overturn of progressive internal waves may be induced in the laboratory, usefully revealing the parameter range and nature of wave breaking, it is unlikely that a sufficiently high representative value of Reynolds number can be obtained to support turbulent mixing following convective overturn and hence to test (7). Laboratory values of $N \sim 2\ \mathrm{s}^{-1}$ and $a \sim 0.02$ m gives $Ra \sim 4 \times 10^8$ but $Re \sim 130, \ll 10^5$. Numerical experiments at sufficiently high Re may, however, soon be feasible.

Laboratory experiments with rotation are needed to determine the internal wave-induced Ri at which KH billows are first observed, Ri_{xc}, and to test (12). The requirement to study breaking internal waves in a rotating system demands sophisticated experimental equipment, design and operation.

c. How to observe internal wave groups and to estimate Λ_I in the ocean?

The identification and tracking of internal wave groups as breaking occurs, and the relatively small speeds of breakers, c_b, pose major measurement problems. Typical values, $N = 10^{-3}\ \mathrm{s}^{-1}$ and $K = 2\pi/100\ \mathrm{m}^{-1}$, give $c_b = N/K \sim 1.6\ \mathrm{cm\ s}^{-1}$. This is comparable to, and often much less, than the mean currents or to the differences between the mean currents in the thermocline and the probable drift of surface platforms; detecting and separating the speed of breaking waves from the background flows will be difficult using moored instruments or measurements from moored or drifting platforms on the sea surface.

The existing observational strategies and platforms to measure internal waves and turbulence that might help obtain data about their relationship fall into the following main classes:

i. Lowered instruments. The most extensive and complete observations of internal waves and breaking (at least of "overturns") are probably those made from R/P *FLIP* by Alford and Pinkel (2000). These are, however, one-dimensional (lowered CTD) whereas Melville and Matusov's (2002) airborne studies of surface wave breaking are two-dimensional. Three-dimensional (3D) measurements are desirable to identify internal wave groups, and to investigate their propagation and characteristics (e.g., see Thorpe, 2010) and, simultaneously, the periodicity and vertical extent of breaking. Some advances toward multidimensional measurements have been made from R/P *FLIP* by simultaneously lowering three temperature recorders at the corners of a horizontal triangle with sides of about 40 m (Pinkel, 1973), and later by lowering two CTDs separated by 20 m (Dr R. Pinkel, SIO; private communication, 2010).

ii. Free-fall probes. These have provided considerable information about the presence, intensity and vertical extent of turbulence (e.g., Winkel *et al.,* 2002) but relatively little about its horizontal scale and persistence or connection to internal waves.

iii. Moored arrays and strings of thermistors. The IWEX trimoored array of 20 current meters (Briscoe, 1975) provided data through which to test the Garrett-Munk spectrum of internal waves but did not have the aim or resolution to observe their breaking. Eriksen's (1978), 8 m high and 20 m in length elongated H-array (the Microscale Sensing Array or MSA), carrying propeller current meters and vertical lines of 7 thermistors, and moored in the main thermocline near Bermuda, provided useful and intriguing information about the variation in time of the Richardson number over periods of as long as 78 h, but little of the connection and structure of waves and turbulence. The NIOZ thermistor strings (van Haren *et al.,* 2001; 2009) have been deployed with as many as 110 thermistors (T-sensors) that are vertically separated by as little as 0.5 m (and could be less). They can record at 1 Hz to a relative accuracy of 0.5 mK for periods of more than a year, and have detected internal waves (van Haren and Gostiaux, 2009) in the Canary Basin and Kelvin-Helmholtz billows (van Haren and Gostiaux, 2010) near the Great Meteor Seamount. Suitably arranged, they appear well suited for intensive 3D studies of waves and turbulence (see Section 6d later; the sensors, each with battery and memory, record individually and are synchronized twice a day). Apart from a small three-dimensional array used in Loch Ness (Thorpe and Hall, 1977) there appear to be no 3D moored array measurements of density structure at 1 m scale.

iv. Towed thermistor chains. The US Naval Research Labs towed "chain" of 180 thermistors vertically spaced by 0.5–0.6 m, from 5 m to 92 m depth, recorded at 20 Hz before averaging to 4 Hz, has been used for 2–3 days at a time in the seasonal thermocline of the Sargasso Sea (Marmorino, 1987; Marmorino *et al.,* 1987). Although demonstrating an apparent link between inertial waves and billows, they provide no information about the across-track scales of temperature structure or the propagation speeds of breakers.

v. Submarine, submersible or AUV-mounted arrays. Billows (Li and Yamazaki, 2001) and turbulence (Osborn and Lueck, 1985; Osborn *et al.,* 1992) have been observed using airfoil probes and vertical thermistor arrays mounted on the bow of the US Navy research submarine "Dolphin." No simultaneous measurements of the horizontal across-track temperature or current variations appear to have been obtained from "Dolphin." Such 3D measurements have been made from thermistors and current meters mounted on rigid spars pushed ahead of a 3-man submersible, the F. A. FOREL, but only in the upper layer of Lake Geneva (Ozen *et al.,* 2006). AUVs have been used to measure turbulence and temperature fluctuations, but the drag imposed on an AUV in carrying a vertical and transverse array would probably be prohibitive.

vi. Free-floating platforms. These have the advantage of (almost) moving with the water and of potentially sensing the relative speed at which breaking waves propagate. Cairns (1975) used

an adapted Snodgrass capsule supporting a vertical 150 m array of 3 Dymec quartz-crystal temperature probes with 10 s response times, sampled at 4 s intervals with a least count precision of ±0.3 mK. The capsule had buoyancy control to allow it to perform vertical oscillations over about 15 m and to track isotherms for periods of about 72 hrs at a depth of 750 m in the eastern N. Pacific 470 km offshore of San Diego in 1973. Waves and apparent overturns of 3–6 m were observed. The RiNo (Richardson number) float devised by Kunze *et al.* (1990a,b) included a vertical array of 8 Thermometric FP14 thermistors with 2 mK precision at 0.5–5 m vertical separation, and 6 acoustic velocimeters at 0.25–5 m vertical separation. It has sampled at 2 min intervals for 9 days at 180–200 m depth in the eastern N. Pacific (PATCHEX area). The float also carried a CTD. It tracked the horizontal water motion to better than 0.25 cm s^{-1} and is closer to being an isopycnal follower than isobar, with an rms vertical flow past the float being ~0.2 cm s^{-1}. The Mixed Layer Lagrangian Float (MLF) devised by D'Asaro *et al.* (1996, who make a very useful study of the compressibility of the float and the extent to which it follows the water motion), is 1.5 m long in the vertical and incorporated a horizontal 1.2 m diameter drag screen to enable it approximately to follow vertical water motions. It carried a pressure sensor and 0.4 mK resolution thermistors at the top and bottom sampled at 0.2 Hz. Its horizontal position was acoustically tracked. Data were collected mainly in the upper ocean mixed layer and in highly turbulent weakly stratified tidal channels (Lien *et al.,* 1998; D'Asaro and Lien, 2000). Here the size of turbulent eddies exceeds the float dimensions and they are tracked by the MLF. In the stratified thermocline, turbulent overturns are often of scale smaller than the MLF (D'Asaro *et al.,* 1996). The rotation of the MLF was used to determine the vertical component of vorticity at the 1 m scale of the drag screen.

vii. Other instruments. Both the free-fall shadowgraph device, SCIMP, used by Williams (1975) and Kunze *et al.* (1987) to investigate double diffusive convective structures in mid-water, and the 3D PIV instruments used to study the structure of turbulent eddies near the seabed (Nimmo Smith *et al.,* 2005; Nimmo Smith, 2008) require substantial power and fixed structures, mirrors, lights or cameras that, without due care, may interfere with the flow. Shear foil probes (Osborn, 1974; Gregg, 1999) generally require a vibration-free platform and a relative current of some tens of centimeters per second and are probably not suited for measurements on free floating platforms.

Acoustics can provide ways to examine small- to medium-scale flow structure and dissipation. Four beam (and even 5 beam) acoustic Doppler Current Profilers are now standard instruments used together with, e.g., thermistor strings (van Haren and Gostiaux, 2009). Moreover, relatively high frequency (100 kHz–1 MHz) sound is scattered by turbulent temperature and salinity microstructure (Thorpe and Brubaker, 1983; Goodman, 1990; Seim *et al.,* 1995; Seim, 1999; Ross and Lueck, 2003). The scattered signal can be used to detect internal waves and billows (Wesson and Gregg, 1994; Armi and Farmer, 2002; Moum *et al.,* 2003). Estimates of the rate of dissipation of turbulent kinetic energy per unit mass, ε, can also be derived from the scattered sound provided that ε is not too great (typically less than about

10^{-6} W kg^{-1}) and that simultaneous measurements of the vertical gradients of temperature and salinity are available (Ross and Lueck, 2005). It is moreover possible to construct robust acoustic sensors to operate at substantial depth, to power sonar transducers and to provide the data storage capacity to record backscatter over periods of a week or more (e.g., Thorpe *et al.,* 1998), a period that could be extended by conditional sampling, e.g., triggered by the detection of high frequency temperature fluctuations.

d. A proposal for new observations

In spite of numerous measurements, some of which are mentioned in part c, there is none other than the photographs taken by Woods (1968) in the seasonal thermocline over 40 years ago that reveals the three-dimensional structure of the ocean at the scales at which dissipation occurs through internal wave breaking, and no measurements of dissipation linked to the presence of breaking wave groups. How might this be remedied?

A rig that could provide many of the required measurements is sketched in Figure 7. It is a 3D, free-floating, neutrally buoyant array of high-resolution thermistors with a CTD, together with orientation, tilt and ADCP to measure relative horizontal currents. The horizontal position of the array is tracked acoustically. The spacing of thermistors should be small enough to resolve overturns[6] (the height of internal breakers) and the relative speed of horizontal advance of breakers (perhaps a horizontal spacing of a few meters). The array should be sufficiently large to detect oceanic fine-structure, resolve 5 m overturns and to estimate the propagation direction and extent of internal breakers, and the vertical and horizontal motion of their parent waves relative to the array, to scales of at least 10 m in the vertical and 10 m in the horizontal. There are already temperature sensors with high resolution, stability and short response times, to provide at least three vertical strings as sketched in Figure 7. Measurements should be made to estimate ε, e.g., from multiple frequency acoustics (in which case a second CTD is required to determine vertical gradients) or from temperature spectra and, in an average way, from the size of overturns. (Powering and recording an airfoil turbulence probe to repeat vertical profiles within the array every minute or so over long periods, might pose insuperable problems.) Deployment is preferably in a location in the main thermocline stable to double-diffusive convection and for periods of at least a month.

Such small-scale 3D observations are needed to obtain insight into the qualitative nature of internal waves, breaking and mixing in the ocean comparable to that conveyed by simply looking at the sea surface, its waves and whitecaps, in high winds—and a quantified image of mid-water mixing that can be used to fuel, inform and stimulate further analytical and numerical investigation of ocean turbulence.

6. The vertical spacing should be sufficient to resolve the Ozmidoz scale, $L_{Oz} = \varepsilon^{1/2}N^{-3/2}$ or, using (15), $L_{Oz} = (K_\rho/\Gamma N)^{1/2}$, which can be evaluated, e.g., using $K_\rho \sim 10^{-5}$ m^{2}s^{-1} and $\Gamma = 0.2$ in a region of historically known N.

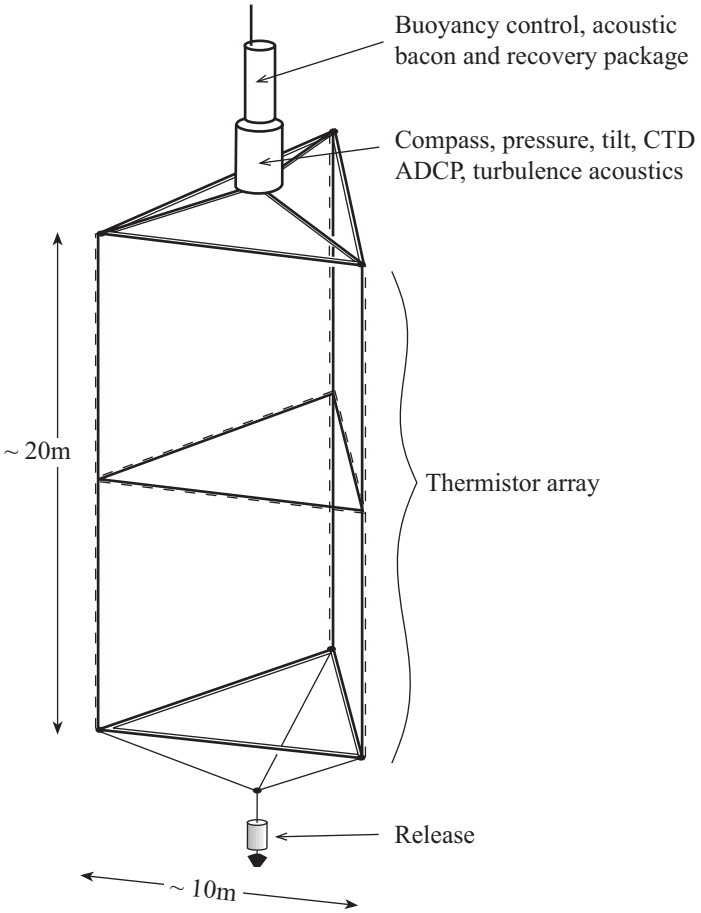

Figure 7. A conceptual sketch of the proposed 3D free-floating array of thermistors to measure internal wave breaking. The temperature sensors, indicated by short bold lines, should be spaced by about 0.25–0.5 m on 3 (or more) vertical cables and at about 1 m on at least one horizontal (triangular) array. The operational depth of the array might be 600–1000 m. As drawn, the array requires some 200–300 temperature sensors.

7. Conclusion

In introducing his chapter on internal waves, Phillips (1966) wrote: "The advances of our understanding of wind-generated waves have been consequent on the exchange between a properly argued theory on the one hand and careful and extensive observations on the other. The problems involved in internal waves are no less complex, but the difficulty of making significant measurements has, to some extent, held back a similarly fruitful interchange." This carefully scripted and understated account of the relative state of knowledge over 40 years ago is still appropriate today. Although measurements of internal waves and theoretical advances, e.g., those in connection with the empirical Garrett-Munk

spectrum in the 1970s and 80s and the HOME-related studies in the 1990s–2000s (Rudnick *et al.,* 2003), have been substantial, there is again a need for the knowledge of internal wave processes, especially their breaking, to emulate the levels attained for surface waves.

In this simplistic discussion of breaking, ignoring factors such as the presence of an "ambient" internal wave field, the radiation of wave energy from internal breakers, and the effects of vertical current shear, we have explored what might be learnt about the dissipation of turbulent kinetic energy resulting from internal wave breaking through convective overturning (Section 3) or shear instability (Section 4) by following the methodology developed for surface wave breaking. Equations are derived for the rate of dissipation of turbulent kinetic energy per unit crest length and per unit breaker height in waves breaking in a group through convective overturn (6) or shear instability (11). A metric, $\Lambda_I(c_b)\mathrm{d}c_b$, is introduced, equal to the area of the fronts of breaking regions, projected onto the vertical and per unit volume, produced by internal breakers traveling at speeds relative to the surrounding fluid between c_b and $c_b + dc_b$. Values of Λ_I necessary to support a vertical diffusivity, K_ρ, of 10^{-5} m^2 s^{-1} are estimated to be of order 1.0×10^{-2} m^{-1} (i.e., a vertical surface area of about 10 cm $\times$ 10 cm in each cubic meter), supposing diffusion is supported by convective overturn or shear instability (Section 5). The metric is also related to the fraction of the thermocline that is turbulent, Q, akin in the surface wave regime to the fractional active whitecap coverage on the sea surface. Several aspects of internal wave breaking are identified which are poorly understood. Some requirements for further research to test and extend the estimates of mixing by breaking internal waves are suggested in Section 6.

Internal waves and surface waves are very different, particularly in their propagation properties (e.g., the relation of $\underline{c}$ and $\underline{c}_g$, and the relative sizes of c_g and the mean flow). Surface waves may be continually forced by the wind. Internal waves generally propagate away from their generation regions and are less likely to be continuously forced; there is usually no local source to re-supply energy lost by breaking. Their propagation properties however depend on N and the mean shear, dU/dz, and may vary substantially over the depth range through which wave groups propagate vertically through the ocean, leading to changes in the waves' stability parameters. The buoyancy frequency, N, in the ocean commonly decreases with increase in depth below the surface mixed layer. Waves propagating downward (conserving their frequency, σ, horizontal wavenumber, k, and vertical energy flux) towards a reflection level where $\sigma = N$, will increase in amplitude ($a \propto (N^2 - \sigma^2)^{-1/4}$), but reduce in slope ($s \propto (N^2 - \sigma^2)^{1/4}$) with an increasing Min Ri_x; the waves become less likely to break. Turbulent mixing associated with such wave groups may be a consequence of their interaction with an ambient field of relatively small internal waves. On the other hand, upward traveling wave groups, perhaps generated by flow over rough topography or as a consequence of wave interactions, become more likely to break. Moreover, the wave slope may increase and wave-induced Richardson number decrease if a critical level is approached as internal waves propagate through a mean shear, dU/dz (Booker and Bretherton, 1967). Complications arise because of the transfer of momentum

with the mean flow. Although also affected by the (horizontal) variation of (surface) currents, surface wave groups are more likely to retain their characteristics during their propagation lifetime.

The direction of travel of breaking surface wave crests is largely determined by the wind direction. It is possible that, measured over a few hours in some chosen location, the direction of propagation of breaking internal waves and the horizontal orientation of breaker fronts, or the major axes of mixed patches of water, have a wide directional spread. We do not know. It is time to renew the study of internal waves and their relation to turbulence. A proposal is made in Section 6d for an instrumented system to make some appropriate measurements.

Acknowledgments. Dr. Ken Melville kindly showed me copies of the two papers by himself and Jessica Kleiss prior to their publication. I am grateful to Mrs. Kate Davis for assistance in preparing the figures, to Professor Alan Davies for use of a computer, and to Dr. Rob Pinkel for advice and comments about an early draft of this paper. Very helpful advice and suggestions were also provided by Drs. Mike Gregg and Hans van Haren. The latter tells me that he presently has about 300 T-sensors, although sadly no funding or program to deploy a high-resolution 3D array.

APPENDIX A

Propagation of the breaking region

If σ is the frequency of a progressive internal wave with wavenumber (k, l, m), in a stationary fluid:

$$\sigma^2 = [(k^2 + l^2)N^2 + f^2m^2]/(k^2 + l^2 + m^2). \tag{A1}$$

The location of a breaking zone in a wave group moves with the vector sum of the phase velocity and the group velocity (Thorpe, 1999a). The breaker speed is therefore

$$\underline{c}_b = \underline{c} + \underline{c}_g = [N^2/(\sigma K)](k, l, mF^2), \tag{A2}$$

where $\underline{c} = (\sigma/K^2)(k, l, m)$ is the phase vector, $\underline{c}_g = [mN^2(1 - F^2)/(\sigma K^4)][km, lm, -(k^2 + l^2)]$ is the group velocity, $K = |(k, l, m)|$ is the wavenumber, and $F = f/N$. This gives

$$c_b = |\underline{c}_b| = NK^{-1}, \tag{A3}$$

which exceeds the phase speed, $c = \sigma K^{-1}$ since $\sigma < N$.

The vector, $\underline{c}_b$, has inclination to the horizontal,

$$\phi = \tan^{-1}(mF^2(k^2 + l^2)^{-1/2}) = \tan^{-1}(F^2/\tan\theta), \tag{A4}$$

where θ is the inclination of the group velocity vector, $\underline{c}_g$, (or of the lines of constant phase) to the horizontal. Since ϕ is small unless $\tan\theta = O(F^2)$, and

$$(\sigma/f)^2 = F^{-2}\sin^2\theta + \cos^2\theta \tag{A5}$$

$\sim F^2 + 1$ if $\tan\theta \sim F^2 \ll 1$, the angle ϕ can only be large if the wave frequency, σ, is very close to the inertial frequency, f.

APPENDIX B

Convective overturn

We first calculate the height of the overturning region as shown in Figure 1 in an internal wave of amplitude a. The equation for the density

$$\rho = \rho_0\{1 - N^2 g^{-1}[z - a\,\sin(kx + mz - \sigma t)]\}, \tag{A6}$$

is an exact solution for progressive waves in the uniformly stratified (incompressible, inviscid and non-diffusive) fluid (Phillips, 1966; Thorpe, 1994b), with wavenumber (k, m) and where ρ_0 is a reference density. A typical profile of the density at $x = t = 0$ when $s = am > 1$ is shown in Figure 2a. At $x = 0$, $t = 0$, the vertical separation of the points A and B at which the vertical density gradient vanishes is given by $2z$ where

$$d\rho/dz = -\rho_0(N^2 g^{-1})[1 - am\,\cos(mz)] = 0, \tag{A7}$$

or

$$z = \eta = \pm m^{-1}\cos^{-1}(s^{-1}), \tag{A8}$$

which is real only if the slope $s \geq 1$; a necessary condition for convective overturn is $s > 1$. The vertical height, h, of the overturning region is therefore

$$h = 2m^{-1}\cos^{-1}(s^{-1}) = 2as^{-1}\cos^{-1}(s^{-1}). \tag{A9}$$

When $1 \leq s \leq 2$ the overturning region is less than the wave height, $2a$, as is evident in Figure 2b (curve a) where $(z_A - z_B) = h$.

[It is assumed here that the overturn is restricted to lie within one vertical wavelength. If $s > 4.604$ (an unlikely occurrence in the ocean), the maximum density at A (z_A) in Figure 1b can exceed the minimum density in the wave below, at the level $-(2\pi m^{-1} + z_A)$, leading to a "collective instability" extending vertically over two waves.]

Other measures of overturn are available. The maximum distance over which the density at point A exceeds that below it, and through which, in a static fluid, it might sink if it could do so without changing its density, is $AC = z_A - z_C$ (Fig. 2a), where

$$mz_A = \cos^{-1}(s^{-1}) \tag{A10}$$

and z_C is the smallest negative root of

$$mz_C - s\,\sin(mz_C) = \cos^{-1}(s^{-1}) - (s^2 - 1)^{1/2}. \tag{A11}$$

Alternatively a "displacement scale" of the maximum density (at level z_A) is equal to the height of A above the "undisturbed density," $\rho = \rho_0(1 - N^2 z/g)$, (the dashed line in Fig. 2a), the distance AD given by

$$m(z_A - z_D) = (s^2 - 1)^{1/2}. \tag{A12}$$

The maximum displacement of fluid from the undisturbed density profile is however the distance EF, where E is the level where the density gradient is equal to that of the undisturbed flow. The vertical coordinate at E is $z_E = \pi/2m$ and F is at $z_F = (\pi/2 - s)/m$, so EF $= s/m = a$, the wave amplitude, as might be expected. The distances AB $= (z_A - z_B) = h$, AC $= (z_A - z_C)$, and AD $= (z_A - z_D)$, each normalized with a, are shown as functions of s in Figure 2b. The chosen value of h, given nondimensionally by curve (a), lies between the two alternatives, (b): $(z_A - z_C)$ and (c): $(z_A - z_D)$. It may be noticed that if the overturning density profile in Figure 2a is "re-ordered" so that the density increases everywhere, a methodology used in calculating the amplitude of overturns in a turbulent flow, the "undisturbed" density profile, $\rho = \rho_0(1 - N^2 g^{-1} z)$, is *not* recovered.[7] The latter *is* recovered, however, by horizontally (or temporally) averaging the disturbed density (A6). Figure A1 shows the vertical density profiles at $x = t = 0$, the re-ordered density profiles and the apparent vertical displacements of the actual profile from the re-ordered when $s = 1.5$ and 2.0. In each case, the maximum apparent displacements, equal to AC in Figure 2a, exceed the wave amplitude, a, as shown by curve b in Figure 2b, and at $s = 2$ they exceed half the vertical wavelength, πm^{-1}.]

A Rayleigh number, Ra, of the overturn can be defined as

$$Ra = N^2(s - 1)h^4(\nu\kappa)^{-1}, \tag{A13}$$

using the density gradient at the centre of an overturning region and h as the characteristic scales, and where ν is the kinematic viscosity and κ is equal to the molecular diffusion of heat, κ_T, or of salinity, κ_S, depending on which property determines the density stratification. Instability and mixing will occur provided Ra exceeds a value that depends on the Prandtl number, $Pr = \nu/\kappa$ (Thorpe, 1994a and b).

Relative to $z = 0$, the potential energy of a column of unit horizontal area at $x = t = 0$ is PE $= \int_{-\eta}^{\eta} g\rho z\, dz$, and substitution for ρ from (A6) and for η from (A8), and integration gives

$$\mathrm{PE} = (N^2\rho_0/12m^3)[24(s^2 - 1)^{1/2} - (mh)^3 - 12mh]. \tag{A14}$$

This is equal to the kinetic energy, $\rho_0 u^2 h/2$, if the velocity fluctuation amplitude, u, is given by

$$u^2 = (Na)^2 G(s), \tag{A15}$$

where

$$G(s) = 2\{3(s^2 - 1)^{1/2} - 3\cos^{-1}(s^{-1}) - [\cos^{-1}(s^{-1})]^3\}[3s^2\cos^{-1}(s^{-1})]^{-1}. \tag{A16}$$

This function is shown in Figure 3.

7. It appears that the formula given by Thorpe (1977; Section 3.1) to find a re-ordered density profile cannot be inverted analytically when (A6) is inserted, but numerical solution is possible and gives the profiles of Figure A1.

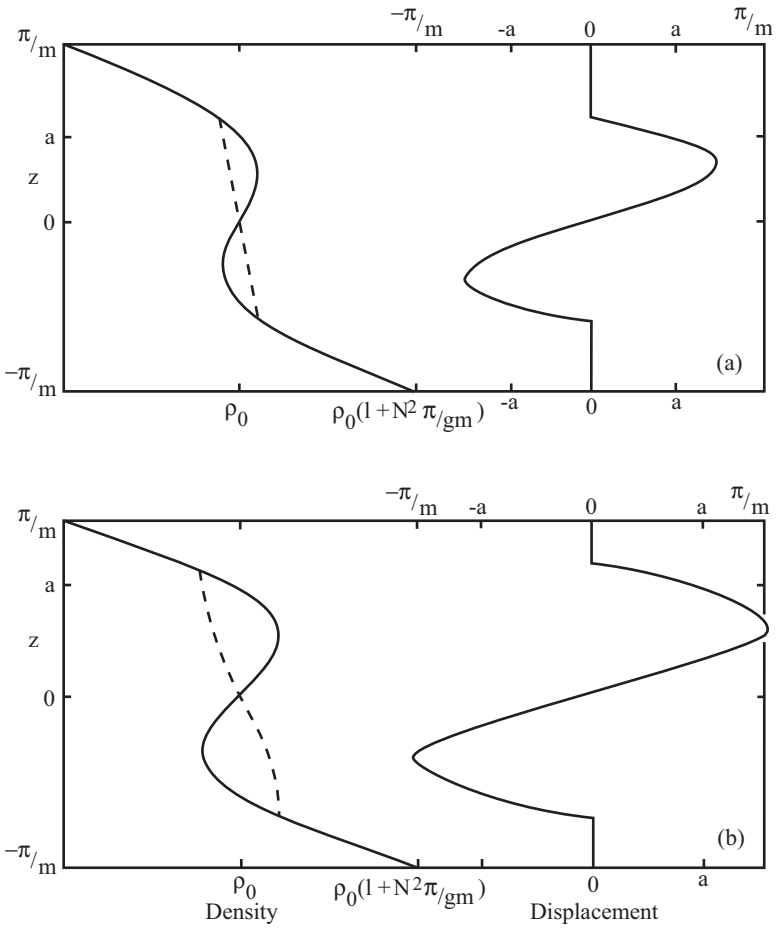

Figure A1. The reordered density profile and "displacement." At the left: the vertical density profiles at $x = t = 0$ (full lines) and the re-ordered density profiles (dashed). At the right: the apparent vertical displacements of the actual density profile from the re-ordered profile, when the wave slope, s, is (a) 1.5 and (b) 2.0. The wave amplitude, $a = s/m$, and half the vertical wavelength, π/m, are indicated (see Appendix B).

APPENDIX C

Dissipation, overturns and the Ozmidov length scale

An alternative, simpler formulation for ε is found by identifying the overturning scale, h, with the Ozmidov length scale, $L_{Oz} = \varepsilon_{Oz}^{1/2} N^{-3/2}$, giving the estimate of the dissipation rate, $\varepsilon_{Oz} = N^3 h^2$. Then, substituting from (A9) and (A15) and using $\varepsilon = q u^3 h^{-1}$:

$$\varepsilon / q\varepsilon_{Oz} = u^3 N^{-3} h^{-3} = s^3 G^{3/2} \{8[\cos^{-1}(s^{-1})]^3\}^{-1}. \tag{A17}$$

This is shown in Figure 3. The function $\varepsilon(q\varepsilon_{Oz})^{-1} \ll 1$, which implies that equating the Ozmidov scale to h probably overestimates the rate of dissipation, ε.

The scale h is, however, substantially greater than the root mean square (rms) "displacement" within the overturning region (e.g., Fig. A1) that, averaged, is generally found to provide a fairly reliable measure of L_{Oz} and hence to estimate the rate of dissipation of turbulent kinetic energy from displacements obtained from vertical CTD profiles. [Suppose, for example, a region of height h is "overturned," conserving mass, in a fluid of density $\rho = \rho_0(1 - N^2g^{-1}z)$ to give a layer of density $\rho = \rho_0(1 + N^2g^{-1}z)$ in $-h/2 \le z \le h/2$. Each density element is displaced by a distance $2z$, so the rms displacement in the overturn is $[\int_{-h/2}^{h/2}(2z)^2dz]^{1/2}h^{-1} = h/6$, substantially less than h.]

The dissipation rate resulting from convective motion following an overturn, ε, is strictly distinct from that required to sustain eddies of height equal to the Ozmidov length scale, ε_{Oz}, in a fluid of mean stable stratification, N. We examine their difference by finding the work done in producing the overturn in $-h/2 \le z \le h/2$ in a fluid of density $\rho = \rho_0(1 - N^2z/g)$ as described above or, equivalently, the turbulent kinetic energy per unit horizontal area that would be produced by the collapse of the unstably stratified layer returning it to its original stratification. The kinetic energy per unit mass, moving each fluid element by a distance $2z$, is

$$\mathrm{KE} = g\rho_0\left[\int_{-h/2}^{h/2}(N^2g^{-1}z)(2z)dz\right](\rho_0h^{-1}),$$

$$= N^2h^2/6.$$

Dissipated in a time, τ, this gives $\varepsilon = N^2h^2/6\tau$. But taking $L_{Oz} = \varepsilon_{Oz}^{1/2}N^{-3/2}$, and $L_{Oz} = h/6$, we find $\varepsilon\varepsilon_{Oz}^{-1} = 6(N\tau)^{-1}$, and the two dissipation rates are equal if $\tau \approx 6N^{-1}$. The assumption that overturns generate turbulent motion that decays at a mean rate ε which is equal to the rate, ε_{Oz}, required to sustain eddies with size equal to the Ozmidov length scale in a stable stratification, N, results in a decay time scale $\tau \approx 6N^{-1}$, that, remarkably, is about equal to that observed (Smyth *et al.,* 1997; see also Appendix D).

APPENDIX D

Mixing through KHI

The x and y component of velocity in an internal wave are

$$u = sk^{-1}\sigma\cos\zeta, \quad v = sk^{-1}f\sin\zeta, \tag{A18}$$

where $\zeta = kx + mz - \sigma t$, and the density is as given in (A6). The x-Richardson number is $Ri_x = (-g/\rho_0)(d\rho/dz)/(du/dz)^2$ or, substituting for u and ρ,

$$Ri_x = (Nk)^2(s\sigma m)^{-2}(1 - s\cos\zeta)(\sin\zeta)^{-2}. \tag{A19}$$

Using (A5):

$$\sigma^2 = N^2(\sin^2\theta + F^2\cos^2\theta), \tag{A20}$$

we have

$$Ri_x = \tan^2\theta[2(\sin^2\theta + F^2\cos^2\theta)]^{-1}(1 - s\cos\zeta)(s\sin\zeta)^{-2}, \tag{A21}$$

If $s < 1$, the Richardson number, Ri_x, is minimum when

$$\cos\zeta = [1 - (1 - s^2)^{1/2}]s^{-1}, \tag{A22}$$

(a value of ζ defined as ζ_0) and its value is then given by

$$\text{Min } Ri_x = \tan^2\theta\{2(\sin^2\theta + F^2\cos^2\theta)[1 - (1 - s^2)^{1/2}]\}^{-1}. \tag{A23}$$

Figure 4 shows the values of s and σ/f at which the minimum Richardson number in the wave-induced flow given by (A23) is equal to $Ri_{xc} = 0.05$, 0.1 and 0.15, values selected as being just sufficient to produce the development of billows, where σ/f is determined from θ using (A5) and $F = 0.1$. With the corresponding values of s and θ, (A21) can be solved to find the two values of ζ at which $Ri_x = ¼$ which surround and are closest to the value of ζ given by (A22). Without loss of generality, we select $x = t = 0$ to obtain values of z given by $\zeta = mz$. These solutions are called z_1 and z_2, and Figure 5 shows the nondimensional values, ζ_0, ζ_1 and ζ_2. It can be shown that $m(z_2 - z_1) = \zeta_2 - \zeta_1 = \cos^{-1}(8Ri_{xc} - 1)$, independent of s.

We may now determine the kinetic energy lost and the potential energy gained if the region z_1 to z_2 is homogenized by mixing:

$$\text{KE} = (\rho_0/2)\left[\int_{z_1}^{z_2}(u^2 + v^2)dz - (\langle u\rangle^2 + \langle v\rangle^2)(z_2 - z_1)\right], \tag{A24}$$

$$\text{PE} = g\left[\int_{z_1}^{z_2} z\rho dz - \langle\rho\rangle\left(\int_{z_1}^{z_2} z dz\right)\right], \tag{A25}$$

where $\langle u\rangle$, $\langle v\rangle$ and $\langle\rho\rangle$ are the mean values of u, v and ρ, respectively, in the range z_1 to z_2. (The vertical velocity, being much less than the horizontal components in near inertial waves, is disregarded in the kinetic energy estimate.) Substitution from (A18) and (A6) gives

$$\text{KE} = (z_2 - z_1)(\rho_0/8)(s\sigma/K)^2\{2(1 + F^2) + (1 - F^2)(\sin 2\zeta_2 - \sin 2\zeta_1)(\zeta_2 - \zeta_1)^{-1} - 4[(\sin\zeta_2 - \sin\zeta_1)^2 + F^2(\cos\zeta_2 - \cos\zeta_1)^2](\zeta_2 - \zeta_1)^{-2}\}, \tag{A26}$$

$$\text{PE} = (z_2 - z_1)(\rho_0/12)N^2m^{-2}[(\zeta_2 - \zeta_1)^2 + 6s(\cos\zeta_2 + \cos\zeta_1) - 12s(\sin\zeta_2 - \sin\zeta_1)(\zeta_2 - \zeta_1)^{-1}]. \tag{A27}$$

The efficiency of mixing or of the transfer of kinetic energy to potential energy is measured by PE/KE. This varies only slightly with s in the range $0 < s < 0.8$, being about 0.13, 0.23 and 0.33 for $Ri_{xc} = 0.05$, 0.1 and 0.15, respectively, and increases by only about 0.03 as s increases from 0.8 to unity. The difference, KE-PE, gives the energy dissipated in turbulent mixing per unit horizontal area. We require the energy lost per unit volume:

$$\Delta = (\text{KE-PE})/(z_2 - z_1) = \rho_0 N^2 m^{-2} A(s, F, Ri_{xc}), \tag{A28}$$

say, where $A(s, F, Ri_{xc})$ is shown in Figure 6. Suppose that the energy is dissipated in turbulence in a time $\tau = rN^{-1}$, where $r \approx 6$ (Smyth *et al.,* 1997),[8] in which the breaking front moves forward a distance $c_b rN^{-1}$, so that, as in Section 3, the mixing occurs over a length $l = rK^{-1}$. The turbulent decay rate is then $\Delta\tau^{-1}$. Using $K = m(\cos\theta)^{-1}$, the rate of dissipation of energy per unit depth and per unit breaker crest length is

$$\varepsilon_I = \rho_0 N^3 m^{-3} A(s, F, Ri_{xc}) \cos\theta. \tag{A29}$$

REFERENCES

Alford, M. and R. Pinkel. 2000. Observations of overturning in the thermocline: The context of ocean mixing. J. Phy. Oceangr., *30,* 805–832.

Andreassen, Ø., P. Ø. Hvidsten, D. C. Fritts and S. Arendt. 1998. Vorticity dynamics in a breaking internal gravity wave. Part 1. Initial instability evolution. J. Fluid Mech., *367,* 27–46.

Armi, L. and D. M. Farmer. 2002. Stratified flow over topography: bifurcation fronts and transitions to the uncontrolled state. Proc. Roy. Soc. Lond. A, *458,* 513–538.

Banner, M. L. and W. L. Peirson. 2007. Wave breaking onset and strength for two-dimensional deep-water wave groups. J. Fluid Mech., *585,* 93–115.

Barad, M. F. and O. B. Fringer. 2010. Simulations of shear instabilities in interfacial gravity waves. J. Fluid Mech., *644,* 61–95.

Booker, J. R. and F. P. Bretherton. 1967. The critical layer for internal waves in a shear flow. J. Fluid Mech., *27,* 513–539.

Briscoe, M. G. 1975. Preliminary results from the trimoored Internal Wave Experiment (IWEX), 1975. J. Geophys. Res., *80,* 3872–3884.

Cairns, J. L. 1975. Internal wave measurements from a midwater float. J. Geophys. Res., *80,* 299–306.

D'Asaro, E. A. and R.-C. Lien. 2000. Lagrangian measurements of waves and turbulence in stratified flows. J. Phys. Oceanogr., *30,* 641–655.

D'Asaro, E. A., D. M. Farmer, J. T. Osse and G. T. Dairiki. 1996. A Lagrangian float. J. Atmos. Ocean. Tech., *13,* 1230–1246.

Donelan, M., M. S. Longuet-Higgins and J. S. Turner. 1972. Periodicity in whitecaps. Nature, *239,* 449–451.

Drazen, D. A., W. K. Melville and L. Lenain. 2008. Inertial scaling of dissipation in unsteady breaking waves. J. Fluid Mech., *611,* 307–332.

8. This time may be compared to the time before the Richardson number at the level, $z_0 = \zeta_0 m^{-1}$, at which breaking sets in with $Ri = Ri_{xc}$, is reduced to the "stable" value, $Ri = \frac{1}{4}$ as a result of wave propagation. Since the wave phase (and the Richardson number field produced by the waves) travels at speed $\sigma K^{-1} = \sigma m^{-1}\cos\theta$ in a direction inclined at an angle θ to the *vertical,* the time taken for the phase line with $Ri = \frac{1}{4}$ to travel from z_1 (at $t = 0$) to z_0 is $(z_0 - z_1)\cos\theta[(\sigma/m)\cos\theta]^{-1} = (\zeta_0 - \zeta_1)N^{-1}(\sin^2\theta + F^2\cos^2\theta)^{-1/2}$ using (A21), or about $3.8N^{-1}$ if $s = 0.6$, $F = 0.1$ and $Ri_{xc} = 0.1$, consistent with $r = O(6)$.

Duncan, J. H. 1981. An experimental investigation of breaking waves produced by a towed hydrofoil. Proc. Roy. Soc. Lond. A, *337,* 331–348.

Eriksen, C. C. 1978. Measurements and models of finestructure, internal gravity waves, and wave breaking in the deep ocean. J. Geophys. Res., *83,* 2989–3009.

Fringer, O. B. and R. L. Street. 2003. The dynamics of breaking progressive interfacial waves. J. Fluid Mech., *494,* 319–353.

Fritts, D. C., S. Arendt and Ø. Andreassen. 1998. Vorticity dynamics in a breaking internal gravity wave. Part 2. Vortex interactions and transition to turbulence. J. Fluid Mech., *367,* 47–65.

Fructus, D., M. Carr, J. Grue, A. Jensen and P. A. Davies. 2009. Shear-induced breaking of large internal solitary waves. J. Fluid Mech., *620,* 1–29.

Garrett, C. 1979. Mixing in the ocean interior. Dyn. Atmos. Oceans., *3,* 239–265.

Garrett, C. and W. Munk. 1972. Oceanic mixing by breaking internal waves. Deep-Sea Res., *19,* 823–832.

Goodman, L. 1990. Acoustic scattering from ocean microstructure. J. Geophys. Res., *95,* 11557–11573.

Grant, H. L., A. Moilliet and W. M. Vogel. 1968. Some observations of turbulence in and above the thermocline. J. Fluid Mech., *34,* 443–448.

Gregg, M. C. 1980. Microstructure patches in the thermocline. J. Phys. Oceanogr., *10,* 915–943.

—— 1989. Scaling turbulent dissipation in the termocline. J. Geophys. Res., *94,* 9686–9698.

—— 1999. Uncertainties and limitations in measuring ε and χ_T. J. Atmos. Ocean. Tech., *16,* 1483–1490.

Gregg, M. C. and T. B. Sanford. 1988. The dependence of turbulent dissipation on stratification in a diffusively stable thermocline. J. Geophys. Res., *93,* 12381–12392.

Kleiss, J. M. and W. K. Melville. 2010. Observations of wave breaking kinematics in fetch-limited seas. J. Phys. Oceanogr., doi:10.1175/2010JPO4383.1 *40,* 2575–2604.

—— 2011. The analysis of sea surface imagery for white cap kinematics. J. Atmos. Ocean. Tech., doi:10.1175/2010JTECH0744.1 *28,* 219–243.

Kunze, E., M. G. Briscoe and A. J. Williams III. 1990a. Interpreting shear and strain from a neutrally buoyant float. J. Geophys. Res., *95,* 18111–18125.

Kunze, E., A. J. Williams III and M. G. Briscoe. 1990b. Observations of shear and vertical stability from a neutrally buoyant float. J. Geophys. Res., *95,* 16127–18142.

Kunze, E., A. J. Williams III and R. W. Schmitt. 1987. Optical microstructure in the thermohaline staircase east of Barbados. Deep-Sea Res., *34,* 1697–1704.

Li, H. and H. Yamazaki. 2001. Observations of a Kelvin-Helmholtz billow in the ocean. J. Oceanography. *57,* 709–721.

Lien, R.-C., E. A. D'Asaro and G. T. Dairiki. 1998. Lagrangian frequency spectra of vertical velocity and vorticity in high-Reynolds-number oceanic turbulence. J. Fluid Mech., *362,* 177–198.

Liu, W., F. Bretherton, Z. Liu, L. Smith, H. Lu and C. J. Rutherford. 2010. Breaking of progressive internal waves: convective instability and shear instability. J. Phys. Oceanogr., *40,* 2243–2263.

Marmorino, G. O. 1987. Observations of small-scale mixing processes in the seasonal thermocline. Part II: wave breaking. J. Phys. Oceanogr., *17,* 1348–1355.

Marmorino, G. O., L. J. Rosenblum and C. L. Trump. 1987. Fine-scale temperature variability: the influence of near-inertial waves. J. Geophys. Res., *92,* 13049–13062.

Melville, W. K. and P. Matusov. 2002. Distribution of breaking waves at the ocean surface. Nature, *417,* 58–63.

Moum, J. M., D. M. Farmer, W. D. Smyth, L. Armi and S. Vagle. 2003. Structure and generation of turbulence at interfaces strained by internal solitary waves propagating shoreward over the continental shelf. J. Phys. Oceanogr., *33,* 2093–2112.

Munk, W. 1966. Abyssal recipes. Deep-Sea Res. *13,* 207–230.

Nimmo Smith, W. A. M. 2008. A submersible three-dimensional particle tracking velocimetry system for flow visualization in the coastal ocean. Limnol. Oceanogr.: Methods, *6,* 96–104.

Nimmo Smith, W. A. M., J. Katz and T. R. Osborn. 2005. On the structure of turbulence in the bottom boundary layer of the coastal ocean. J. Phys. Oceanogr., *35,* 72–93.

Orlanski, I. and K. Bryan. 1969. Formation of the thermocline step structure by large-amplitude internal gravity waves. J. Geophys. Res., *74,* 6975–6983.

Osborn, T. R. 1974. Vertical profiling of velocity microstructure. J. Phys. Oceanogr., *4,* 109–115.

—— 1980. Estimates of the local rate of vertical diffusion from dissipation measurements. J. Phys. Oceanogr., *10,* 83–89.

Osborn, T. R. and R. G. Lueck. 1985. Turbulence measurements from a submarine. J. Phys. Oceanogr., *15,* 1502–1520.

Osborne, T. R., D. M. Farmer, S. Vagle, S. A. Thorpe and M. Cure. 1992. Measurements of bubble plumes and turbulence from a submarine. Atmos. Ocean, *30,* 419–440.

Ozen, B., S. A. Thorpe, U. Lemmin and T. R. Osborn. 2006. Cold-water events and dissipation in the mixed layer of a lake. J. Phys. Oceanogr., *36,* 1928–1939.

Phillips, O. M. 1966. The Dynamics of the Upper Ocean, Cambridge University Press, 261 pp.

—— 1985. Spectra and statistical properties of the equilibrium range in wind-generated gravity waves. J. Fluid Mech., *156,* 505–531.

Pinkel, R. 1975. Upper ocean internal wave observations from FLIP. J. Geophys. Res., *80,* 3892–3910.

Polzin, K. 1996. Statistics of the Richardson number: mixing models and finestructure. J. Phys. Oceaonogr., *26,* 1409–1425.

Ross, T. and R. Lueck 2003. Sound scattering from ocean turbulence. Geophy. Res. Lett., *30,* 1343, doi:10.1029/2002GL016733.

—— 2005. Estimating turbulent dissipation rates from acoustic backscatter. Deep-Sea Res. I, *52,* 2353–2365.

Rudnick, D. L., T. Boyd, R. E. Brainard (and 16 others). 2003. From tides to mixing along the Hawaiian Ridge. Science, *301,* 355–357.

Seim, H. E. 1999. Acoustic backscatter from salinity microstructure. J. Atmos. Oceanic Technol., *16,* 1491–1498.

Seim, H. E., M. C. Gregg and R. T. Miyamoto. 1995. Acoustic backscatter from turbulent microstructure. J. Atmos. Ocean. Tech., *12,* 367–380.

Shih, L. H., J. R. Koseff, G. N. Ivey and J. H. Ferziger. 2005. Parameterization of turbulent fluxes and scales using homogeneous sheared stably stratified turbulence simulations. J. Fluid Mech., *525,* 193–214.

Smyth, W. D., P. O. Zavialov and J. N. Moum. 1997. Decay of turbulence in the upper ocean following sudden isolation from surface forcing. J. Phys. Oceanogr., *27,* 810–822.

Staquet, C. and J. Sommeria. 2002. Internal gravity waves: from instabilities to turbulence. Annu. Rev. Fluid Mech., *34,* 559–593.

Thorpe, S. A. 1977. Turbulence and mixing in a Scottish loch. Phil. Trans. Roy. Soc. Lond. A, *286,* 125–181.

—— 1994a. The stability of statically unstable layers. J. Fluid Mech., *260,* 315–331.

—— 1994b. Statically unstable layers produced by overturning internal gravity waves. J. Fluid Mech., *260,* 333–350.

—— 1999a. On internal wave groups. J. Phys. Oceanogr., *29,* 1085–1095.

—— 1999b. On the breaking of internal waves in the ocean. J. Phys. Oceanogr., *29,* 2433–2441.

—— 2002. On the dispersion of pairs of internal inertial gravity waves. J. Mar. Res., *60,* 461–476.

—— 2010. The relation between the duration and shape of internal wave groups. J. Mar. Res., *68,* 63–95.

Thorpe, S. A. and J. M. Brubaker. 1983. Observations of sound reflection by temperature microstructure. Limnol. Oceanogr., *28,* 601–613.

Thorpe, S. A. and A. J. Hall. 1977. Mixing in upper layer of lake during heating cycle. Nature, *265,* 719–722.

Thorpe, S. A., M. J. Ulloa, D. Baldwin and A. J. Hall. 1998. An Autonomously Recording Inverted Echo Sounder; ARIES II. J. Atmos. Ocean. Tech., *15,* 1347–1361.

Tian, Z., M. Perlin and W. Choi. 2010. Energy dissipation in two-dimensional unsteady plunging breakers and an eddy viscosity model. J. Fluid Mech., *655,* 217–257.

Troy, C. D. and J. R. Koseff. 2005. The instability and breaking of long internal waves. J. Fluid Mech., *543,* 107–136.

van Haren, H. and L. Gostiaux. 2009. High-resolution open-ocean temperature spectra. J. Geophy. Res., *114,* C05005, doi:10.1029/2008JC004967,2009.

van Haren, H. and L. Gostiaux. 2010. A deep-ocean Kelvin-Helmholtz billow train. Geo. Res. Letts, *37,* L03605, doi:10.1029/2009GL041890, 2010–10-27.

van Haren, H., M. Laan, D.-J. Buijsman, M. G. Smit and E. Keijzer. 2009. NIOZ3: independent temperature sensors sampling yearlong data at a rate of 1 Hz. IEEE J. Ocean Eng., *34,* 315–322.

van Haren, H., R. Groenewegen, M. Laan and B. Koster. 2001. A fast and accurate thermistor string. J. Atmos. Ocean. Tech., *18,* 256–265.

Wesson, J. C. and M. C. Gregg. 1994. Mixing at the Camarinal Sill in the Strait of Gibraltar. J. Geophys. Res., *99,* 9847–9878.

Williams III, A. J. 1975. Images of ocean microstructure. Deep-Sea Res., *22,* 811–829.

Winkel, D. P., M. C. Gregg and T. B. Sanford. 2002. Patterns of shear and turbulence across the Florida Current. J. Phys. Oceanogr., *32,* 3269–3285.

Woods, J. D. 1968. Wave-induced shear instability in the summer thermocline. J. Fluid Mech., *32,* 791–800.

Wunsch, C. and R. Ferrari. 2004. Vertical mixing, energy and the general circulation of the oceans. Annu. Rev. Fluid Mech., *36,* 281–314.

Received: *24 August, 2010;* revised: *3 December, 2010.*